ACS SENSORS

pubs.acs.org/acssensors Article

An Integrated Food Freshness Sensor Array System Augmented by a Metal−Organic Framework Mixed-Matrix Membrane and Deep Learning

Peihua Ma, Wenhao Xu, Zi Teng, Yaguang Luo, Cheng Gong, and Qin Wang*

Cite This: *ACS Sens.* 2022, 7, 1847−1854 Read Online

ACCESS | Metrics & More | Article Recommendations | Supporting Information

ABSTRACT: The static labels presently prevalent on the food market are confronted with challenges due to the assumption that a food product only undergoes a limited range of predefined conditions, which cause elevated safety risks or waste of perishable food products. Hence, integrated systems for measuring food freshness in real time have been developed for improving the reliability, safety, and sustainability of the food supply. However, these systems are limited by poor sensitivity and accuracy. Here, a metal−organic framework mixed-matrix membrane and deep learning technology were combined to tackle these challenges. UiO-66-OH and polyvinyl alcohol were impregnated with six chromogenic indicators to prepare sensor array composites. The sensors underwent color changes after being exposed to ammonia at different pH values. The limit of detection of 80 ppm for trimethylamine was obtained, which was practically acceptable in the food industry. Four state-of-the-art deep convolutional neural networks were applied to recognize the color change, endowing it with high-accuracy freshness estimation. The simulation test for chicken freshness estimation achieved accuracy up to 98.95% by the WISeR-50 algorithm. Moreover, 3D printing was applied to create a mold for possible scale-up production, and a portable food freshness detector platform was conceptually built. This approach has the potential to advance integrated and real-time food freshness estimation.

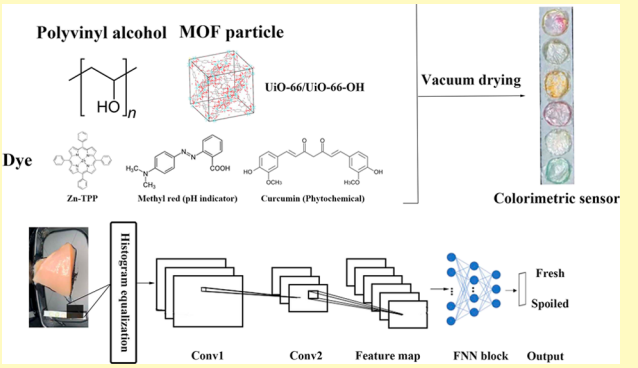

KEYWORDS: *real-time estimation, metal−organic frameworks, ammonia, deep convolutional neural networks, UiO-66*

Food labels currently used in the food industry only provide consumers with rough guidance to their expected shelf-life since manufactories assume that the products are exposed to a limited set of predefined storage conditions.[1] The static nature of these labels brings up two major challenges: (a) they do not take into consideration variant conditions that reduce shelf-life, such as temperature abuse and the difference between batches,[2] and (b) perishable food waste caused by the overcautious allocation of the expiration date accounted for approximately 35% of the annual production, according to a working paper from the United States Department of Agriculture (USDA).[3] Therefore, novel analytical tools that are able to determine the quality and safety attributes in real time and accurately estimate the shelf life of food products may potentially contribute to market value as well as sustainable development.

Ideally, real-time shelf life prediction for foods should satisfy the following requirements:[1,2,4] (a) the complexity of natural foods requires the detection system to input multiple attributes' indicators for shelf-life estimation; (b) indicators and sensors should reliably monitor the signals originating from actual deterioration of the product; (c) integration of in situ computing should determine the current freshness and estimate the shelf life in real time. At present, the mainstream approach is to mimic the mammalian olfactory system to develop an artificial scent screening system, which has been applied in the detection of drugs, explosives, and rapid food analysis. However, considering that the kinetics of the food deterioration process are influenced by multiple factors, such as nutritional loss, microbial growth, environmental factors, etc., conventional methods that integrate metal oxides or colorimetric dyes into a cross-reactive sensor array suffer from poor sensitivity and low accuracy.[5−7] To address these challenges, we took advantages of reticular chemistry, metal−organic framework mixed-matrix membrane (MOF-MMM),

Received: February 1, 2022
Accepted: July 4, 2022
Published: July 14, 2022

with help from deep learning technology to achieve practical and acceptable accuracy for food freshness estimation systems.

Metal−organic frameworks (MOFs), a family of chemically mutable materials with high porosity, offer various advantages and thus are considered as promising additives for mixed-matrix membranes (MMMs).[8] The chemically diverse and controllable MOF structures (by careful selection of ligands with appropriate chemical functionalities) can be prepared to enhance the interactions with bulk polymeric materials, which improve the selectivity of MMMs by reducing the microgaps between inorganic and organic phases.[9] Furthermore, the chemical mutagenicity of MOFs can be leveraged to enhance adsorption selectivity to certain chemical species.[10] In recent years, MOF-based materials have been widely investigated in the development of food safety sensors due to advantages of uniform structures, easy-to-functionalize surfaces, tunable composition, ultrahigh porosity for the detection of pesticide residues, veterinary drugs, pathogens, heavy metals, mycotoxins, and illegal additives, etc.[5,11,12] Stability is one of the major concern for MOF application in food application; nevertheless, UiO-66, which has high structural robustness, is one of several potential MOFs. UiO-66 has excellent thermal and chemical stability in water, even stable in very acidic aqueous solutions, and demonstrated a high adsorption capacity for polar analytes.[13] However, accurate image recognition of MMMs is highly challenging with traditional statistical methods, including principal component analysis (PCA) and hierarchical cluster analysis (HCA).[12] The latest breakthroughs in computer vision research proved the deep convolutional neural network (DCNN) and its derivative algorithms as a promising approach for image recognition, and they have exhibited superiority in dietary monitoring, food supply chain evaluation, and food quality detection.[4,5]

Here, the MOF-MMM system was for the first time introduced to prepare a food freshness sensor array. When compared to other materials, e.g., an organic polymer membrane sensor array or inorganic membranes, a balance between production cost, gas selectivity, and stability is obtained by the MOF-MMM system. MOF-MMM was synergized to overcome the low sensitivity, and DCNN technology was applied to improve the accuracy of the cross-reactive colorimetric sensor array system. The UiO-66-OH/PVA MOF-MMM system was developed and systematically characterized. Moreover, a real-time sensor array fingerprint pattern recognition by DCNN was optimized after the comparison of four state-of-the-art DCNN models. Finally, we integrated the MOF-MMM sensor and DCNN image recognition system together to achieve the prediction of chicken freshness with an accuracy of up to 98.95%.

EXPERIMENTAL SECTION

Materials. Zirconium tetrachloride (99.5%), 2-hydroxyterephthalic acid (BDC-OH, 98.0%), *N*,*N*-dimethylformamide (DMF, 99.0%), Nile red, poly(vinyl alcohol) (PVA, M_w 85,000−124,000), acetic acid (HAc, 99.9%), boric acid, (99.8%), 2-methoxyethanol (99%), and 6 dyes, i.e., methyl red (MR), 5,10,15,20-tetraphenyl-21*H*,23*H*-porphine zinc (Zn-TPP), curcumin (CUR), chlorophenol red (CPR), bromocresol purple (BCP), and bromophenol blue (BPB), ammonia hydrogen solution (25% in water), methylamine solution (33% in absolute ethanol), and trimethylamine solution (45% in water) were purchased from Sigma-Aldrich (St. Louis, MO, USA). Detailed compositions of dyes used in this study are presented in Table S1. All chemicals are of analytical grade. The chicken breast was bought from Costco Wholesale Corporation (Seattle, WA, USA). The ZipBag was bought from a local market (Ziploc, NJ, USA).

Synthesis of UiO-66 and UiO-66-OH. UiO-66-OH was synthesized by a solvothermal method following a previous report with modification.[14] First, $ZrCl_4$ (1.17 g, 5 mmol), BDC (0.83 g, 5 mmol), and 1.0 mL of acetic acid were dissolved in DMF (30 mL) at room temperature. The UiO-66 particle was synthesized by replacing BDC with BDC-OH (0. 92 g, 5 mmol). After adding 2 mL of deionized water and thoroughly mixing the mixture, it was placed in a Teflon-lined stainless-steel autoclave. The autoclave was heated at 121 °C on an oil bath. After cooling the solution for 30 min at room temperature, the UiO-66 and UiO-66-OH particles were separated by centrifugation (12,096*g*, 10 min) at room temperature and washed three times with ethanol. The resultant white powder was baked in a 40 °C oven for 4 h before being verified using XRD and SEM.

Synthesis of Dye@UiO-66/PVA and Dye@UiO-66-OH/PVA MMM. PVA resin (1 g) was first dissolved in deionized water at 90 °C for 1 h with stirring to obtain 10 wt % PVA aqueous solution. To avoid aggregation, UiO-66 or UiO-66-OH nanoparticles (200 mg) were first dispersed in 50 mL of water with assistance from ultrasound. A certain volume of the prepared MOF dispersion was diluted with deionized water to a final volume of 27 mL. Subsequently, 2.5 mL of PVA aqueous solution and 0.5 mL of dye solution (e.g., 5 mg/mL in 2-methoxyethanol) were added to it. After vigorous stirring, 0.2 mL of each solution was transferred to its assigned well on a 96-well plate, with a diameter of 6 mm for each pore. The solution was then degassed and dried in a vacuum for 24 h on a 96-well plate. To make the sensor array, all of the films with various colors were taped together on paper tape.

Calculation of Amine Gas Concentration. Experiments on amine gas detection were carried out in conventional Petri dishes (100 × 15 mm) at a temperature of 20 °C. The colorimetric sensor array was attached to the Petri dish's lid. A particular volume of liquid analyte (i.e., ammonia (NH_3), methylamine (MA), and trimethylamine (TMA)) was injected into the dish and sealed with parafilm to achieve the desired gas concentration. The resulting gas concentration (C) (ppm) was calculated using eq 1

$$C = \frac{V \times D \times W}{M \times V} \times 22.4 \times 10^7 \quad (1)$$

where V (μL) is the liquid analyte volume, D (mg/L) is the liquid density, W is the mass fraction of the liquid, M (g/mol) is the molecular weight of the liquid analyte, and V (L) is the volume of Petri dishes.

Determination of the Swelling Index. When the polymer matrix was submerged in water, the swelling index was utilized to assess each membrane's capacity to swell. Initially, each film was weighed (M_{dry}). The films were then soaked in room temperature water. Each membrane was removed from the water and weighed on a regular basis until a consistent membrane weight ($M_{swollen}$) was achieved, indicating that equilibrium had been established. The swelling index of films or water uptake was determined by eq 2[15]

$$\text{swelling index}(\%) = \left(\frac{M_{swollen} - M_{dry}}{M_{dry}}\right) \times 100\% \quad (2)$$

Solubility Determination for MOF/PVA-MMM. Each film's membrane sample was dried in an oven at 100 °C for 24 h. The membranes were then weighed to determine their original dry content (W_i). After that, all membrane samples were immersed in water and kept at 30 °C in a covered beaker for 24 h while being stirred. The membrane samples were then removed, washed, and dried in an oven at 100 °C until they reached a consistent weight (W_0). Membrane solubility was determined by eq 3[15]

$$\text{solubility}(\%) = \left(\frac{W_i - W_0}{W_i}\right) \times 100\% \quad (3)$$

Total Volatile Basic Nitrogen (TVB-N) Measurement. Fresh chicken breast (200 ± 30 g), without any preparation, was put in a

https://doi.org/10.1021/acssensors.2c00255
ACS Sens. 2022, 7, 1847−1854

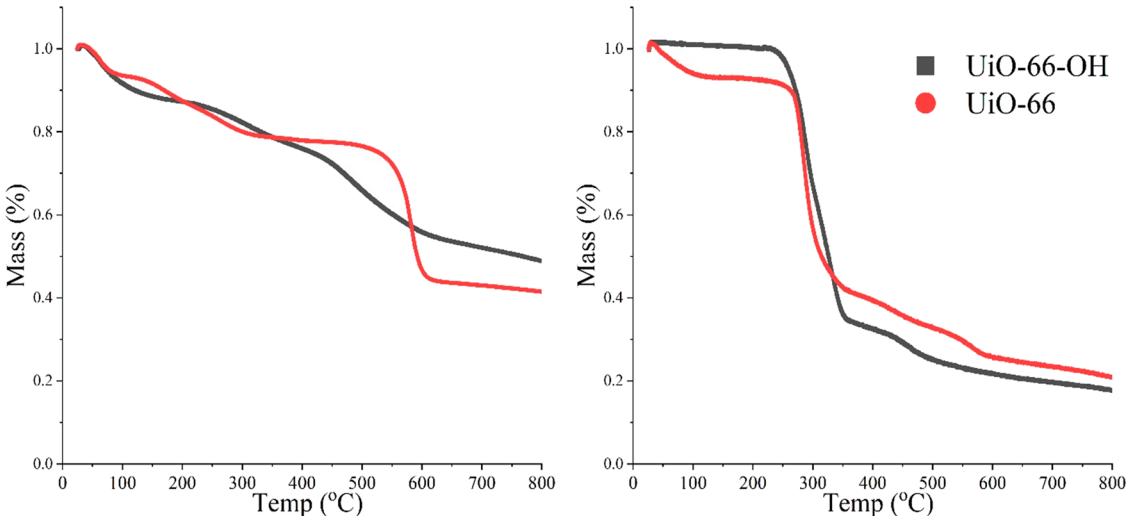

Figure 1. Thermogravimetric analyses of NPs of UiO-66 and UiO-66-OH (left) and films of UiO-66/PVA and UiO-66-OH/PVA (right).

plastic box to replicate store storage conditions. Each package has one sensor array affixed to the inside of the box. Before analysis, the chicken was kept at 4 °C.

A separate batch of 24 (8 storage periods × 3 parallel studies) packets of chicken was created for TVB-N testing to examine the freshness of chicken without the interference of picture capture. 100 mL of distilled water was used to homogenize 10 g of minced chicken (Ultra-Turrax T25, IKA, Staufen, Germany). After 30 min, the mixture was filtered to get a liquid sample. Then, in the inner chamber of the Conway dish, 3 mL of boric acid absorption solution (20 g/L) and 50 mL of pH indicator (methyl red:bromocresol green = 1:5, v/v) were added (diameter 90 mm). 3 mL of potassium carbonate saturated solution and 1 mL of sample liquid were introduced to the outer chamber in that order. The Conway dish was sealed and incubated for 2 h at 37 °C. As an absorbent solution, boric acid absorbed the volatile amine vapors. 0.1 mol/L hydrochloric acid (HCl) was used to titrate the abovementioned combination. The inner volume of the Conway dish after airtight sealing is 100 mL. The number of volatile amines was calculated with eq 4

$$X = \frac{(v1 - v2) \times C \times 14}{m \times 0.05} \times 100 \quad (4)$$

where X is TVB-N level of the sample (mg/100 g), $v1$ is the volume of 0.1 mol/L HCl consumed by the sample (mL), $v2$ is the volume of 0.1 mol/L HCl consumed by the control (mL), C is the concentration of HCl (mol/L), 14 is the atomic mass of nitrogen (g/mol), and m is the weight of the sample (g).

Circular Region of Interest (CROI) Identification. To detect the color region of the sensor array, the Hough circle transformation was used. By "voting" in the Hough parameter space and then picking global maxima in an accumulator matrix, the circled candidates were created. The inverse ratio of the resolution was set to 1, the higher threshold for the internal Canny edge detector was set to 15, the threshold for center detection was set to 13, and the radius range to be detected was set to [20,40) pixels to get the best result. The CROI was calculated using the Hough circle transform to designate seven dye regions.

Database Preparation. To capture data from the sensor, a 5 s video was shot with chicken at a specific storage period for each box. The color and intensity of the backdrop light in the photo box changed throughout the course of 5 s, depending on the software parameters. Eight time periods covering the spoiling process were chosen. A piece of chicken was tested for TVB-N throughout the data collection time, while others were utilized for picture capture. We altered the light in the input photographs and photographed them using an iPhone 11 Max Pro for training to completely simulate real-world circumstances. Also, to further mimic the lighting conditions in the real world, the light intensity and color temperature of the sample photo area will be continuously changed during the collection process. Images collected in this study included both the chicken and sensor. The 60 fps video was then randomly sampled at 10 fps and exported as an image set. Based on the actual measured TVB-N results and chicken freshness criteria, we labeled samples <28 mg N/100 g as fresh and > 28 mg N/100 g as spoiled followed by a previous study in food research and industry.[16] Finally, the database was divided into a training set and a testing set in a 7:3 ratio. The test set had 1927 pictures, and the final training set had 4492 tagged images. In both the training and test sets, the fresh to spoilt ratio was 1:1.

Statistical Analysis. Measurements of particle size, surface charge, swelling index, and solubility were performed in triplicate with data reported as mean ± standard error. Data were analyzed by one-way analysis of variance at a significance level of $p = 0.05$ using the SPSS 16.0 package (SPSS Inc., Chicago, USA).

RESULTS AND DISCUSSION

Synthesis and Morphologies of the UiO-66-OH/PVA Sensor Array. The identification of MOF-MMM materials and the detail of UiO-66-OH NP characteristics are comprehensively reported in the Supporting Information.

XRD was first utilized to examine the MOF particle and MOF-MMM system, and the results showed the same diffraction results for both UiO-66 and UiO-66-OH, which exhibited a distinct crystal peak in the detect range (Figure S1). However, when prepared as a MOF-MMM system, only the PVA peak was detected, a result consistent with other MOF-MMM-related reports. The results of the thermogravimetric analysis are shown in Figure 1. The UiO-66 NPs were decomposed at 550−600 °C, but UiO-66-OH NPs started to decompose from 400 °C, without a clear decomposition stage. This was due to the defects brought by the hydroxyl groups, which affected the stability of MOF structures. For the MOF-MMM film system, the thermogravimetric analysis showed decomposition in the range of 250−300 °C, which is the thermal decomposition temperature of PVA. This result showed that the factor affecting the thermal stability of the system is mainly PVA. Also in the interval less than 100 °C, there was a 10% mass loss in the MMM prepared with UiO-66-OH since it binds more readily to water in the environment than the MMM prepared with bare UiO-66, resulting in a bigger mass loss due to volatilization of absorbed water during thermogravimetric analysis.

https://doi.org/10.1021/acssensors.2c00255
ACS Sens. 2022, 7, 1847−1854

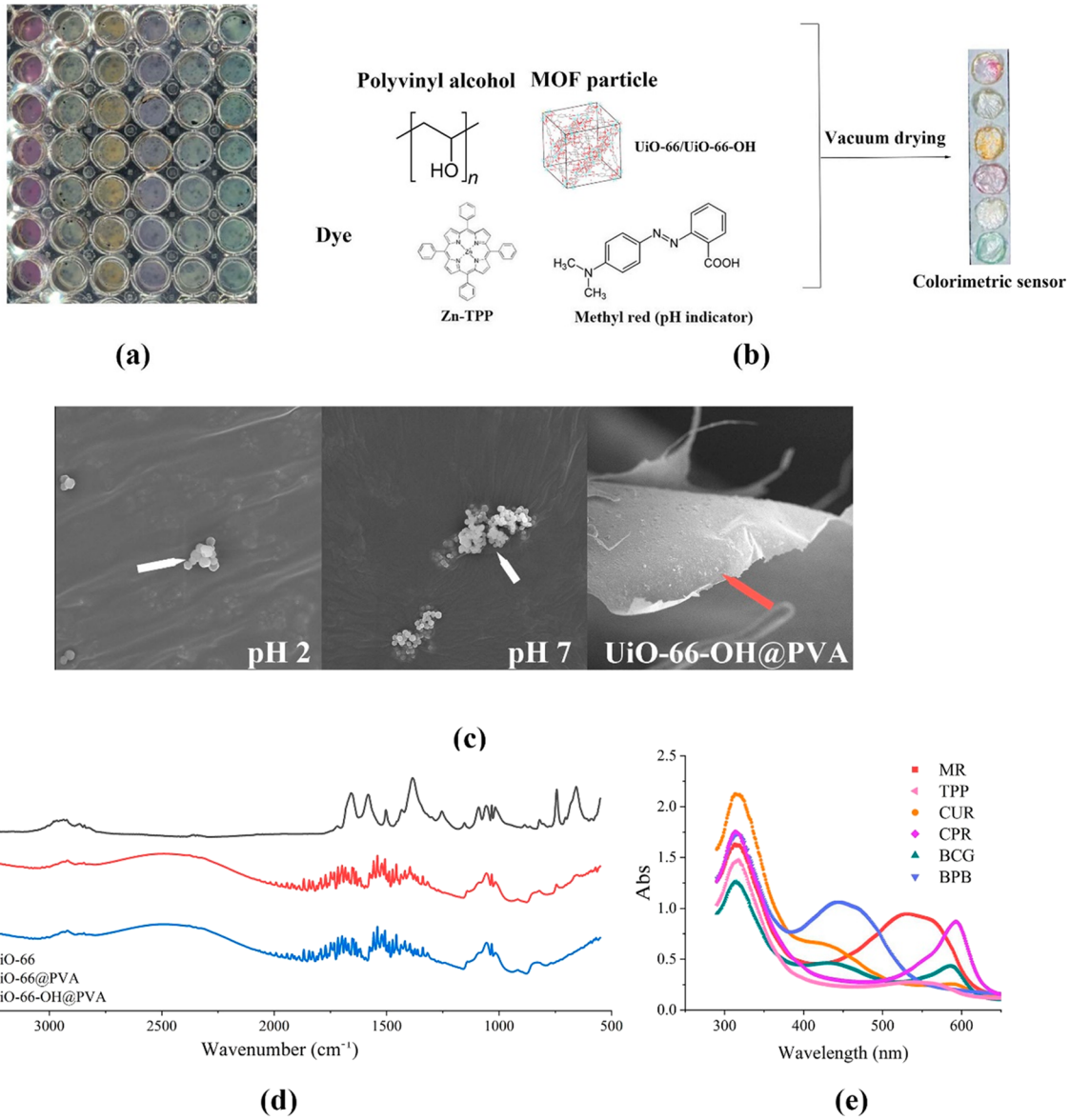

Figure 2. Preparation and characterization of colorimetric sensor array. (a) Schematic of the sensor array in 3D printing molds. Each pore filled with six types of dyes with UiO-66-OH/PVA solution. (b) Schematic showing the fabrication of the dye@UiO-66-OH/PVA sensor array. UiO-66-OH are cross-linked with PVA via hydrogen bonding, and the dye was adopted to the surface of UiO-66-OH. (c)Scanning electron microscopy image of UiO-66-OH NPs at pH 2 (left), UiO-66-OH NPs at pH 7 (middle), and the UiO-66-OH/PVA film. (d) Infrared spectra of UiO-66 NPs, the UiO-66@PVA film, and the UiO-66-OH@PVA film. (e) Spectral scanning of the six different dyes loaded in the UiO-66-OH@PVA film. Scanning range from 300−650 nm.

The UiO-66-OH/PVA film loaded with three categories of dyes was successfully synthesized (Figure 2a). The MMM system was directly formed on the PARAFILM M film by using a 3D-printed mold, which achieved a low cost and had potential for mass production (schematic of sensor array fabrication shown in Figure 2b). To deposit the gas-sensitive sensors on parafilm, six 100 μL dye@UiO-66-OH/PVA solutions were drop-cast onto the pore of the mold, where the diameter of each pore was 6 mm and the distance between neighboring pores averages at 2 mm. Many studies have proved the reliance of gas transfer efficiency and sensing stability on the microstructure and affinity to dyes of the nanocomposites.[4,17] SEM was applied to observe the morphologies of the MOF particles at acidic to neutral pH values as shown in Figure 2c. The uniform MOF NPs kept their crystal structure with a particle size of approximately 100 nm, and there were no observed changes for MOF NPs in different pH conditions. Meanwhile, no dye aggregation was found in the SEM images, indicating that MOF NPs play a critical role as a carrier in dispersing the dye, which was demonstrated in previous reports. Such a porous structure was expected to provide a large surface area and gas sensing site. Figure 1d shows the FTIR spectrum of MOF NPs and MOF MMMs. Peaks related to O−H and C−H bending were intermingled with the Zr−O peak at lower frequencies (main bands at 746 cm^{-1}). The longitudinal and transverse peaks were assigned to a twin peak at 725 and 620 cm^{-1}, respectively. Peaks related to O−H and C−H bending were intermingled with the Zr−O peak at lower frequencies (main bands at 746 cm^{-1}). The longitudinal and transverse peaks were assigned to a twin peak at 725 and 620 cm^{-1}, respectively. The MOF showed absorption bonds at 1590 and 1390 cm^{-1} that were

https://doi.org/10.1021/acssensors.2c00255
ACS Sens. 2022, 7, 1847−1854

assigned to the −COOH groups. The aromatic region (C═C) of the methyl red dye appeared at 1445 cm^{-1}.

The maximum absorption peaks of the different dyes were detected using UV−Vis (Figure 2e). They were in the visible range of 400−650 nm, which indicated that the sensor color was effectively extracted using a CCD camera in the visible band of the mobile device. At the same time, the characteristic peaks of each dye were clearly visible, which indicated that the MOF-MMM system itself had little interference with the color.

To test its ability to satisfy the character requirement as a food package in practical conditions, water stability, thermal stability, and mechanical properties were characterized. First, dye leakage and the swell index were tested by immersing Nile red-loaded UiO-66-OH/PVA films (NR@UiO-66-OH/PVA) in water using a Nile red-loaded PVA film (NR@PVA) as the control group. The swelling index and solubility of the sensor array are presented in Figure 3. Nile red was selected as a model dye since it has a characteristic absorbance peak at 580 nm at pH 6.3, which is in the working range of the sensor array. UiO-66-OH/PVA showed a significantly higher swelling index (24%) than the PVA film. Previous studies reported that PVA showed a strong pH-dependent swelling behavior, having a swelling ratio index in the range of 5%−15% when the pH was in the range between 4 and 7 at room temperature. After being mixed with UiO-66-OH NPs, the water retention capability was slightly increased due to the hydroxyl groups on MOF NPs. Considering the robust water stability of UiO-66 NPs, the MOF MMM intelligent packaging film had a practical acceptable swelling ratio.[15] Furthermore, the solubility of the different systems was also tested. For the UiO-66-OH/PVA system, the supernatant had no visible color and negligible absorbance at 580 nm, whereas NR@PVA showed a red supernatant. Furthermore, with the increased immersion time, the absorbance increased from 0.7 to 2.1. These results indicated that MOF NPs prevented Nile red from leaking out of the MMM, whereas weak van der Waals force between PVA and Nile red could not prevent the leakage, which may ensure the package safety of the sensor array system.

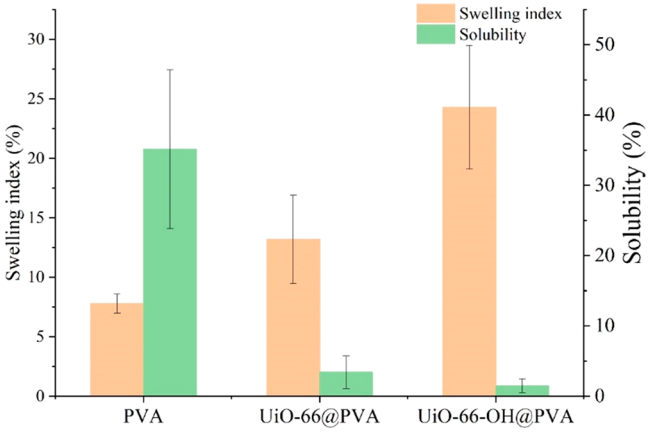

Figure 3. Swelling index (%) and solubility of the PVA film with two MOF-MMM films in an aqueous environment.

Validation and Sensitivity of MOF-MMM in Standard Conditions. Proteins are microbially degraded into peptides and free amino acids, which are further decomposed into low-grade amines and ammonia. The latter may be used as vital indicators in meat and seafood safety. To evaluate and optimize the sensing performance of MOF-MMM, dye@UiO-66-OH/PVA, dye@UiO-66/PVA, and dye@PVA were exposed to methylamine (MA) gas. The sensor array exhibited an obvious pattern change over the test time with increasing concentration of MA (Figure 4a). Dye@UiO-66-OH/PVA and dye@UiO-66/PVA exhibited visible color differences with increased MA concentration. These results demonstrated the potential of our approach in rapid identification and quantification of VOCs from foods. Limited by the human naked eye's color distinguish ability, this result could not be clearly separated by our eyes, but nowadays cell phone cameras can clearly distinguish colors.[5] To quantitatively describe the sensor array response, the Euclidean distance (ED) of the circular region of interest (CROI) RGB value was measured under exposure to different MA concentrations and different time periods (Figure 5). The RGB values exhibited by the sensor array were retrieved using the Hough circle transform technique by an image recognition and color extraction system. To sum, a circle candidate region was created by "voting" in the Hough parameter space and then sorting the global maximum from an accumulator matrix to segment the CROI from a sensor array picture. Figure 4b depicts the perimeter of the segmented CROI. Then, 50 pixels were chosen at random from each CROI and labeled with the dye's name, and the variance of each pixel's color components was estimated. During the different exposure times, the time-dependent pattern change was attributed to the increase of the reaction process since our setup allows temporal accumulation of VOCs

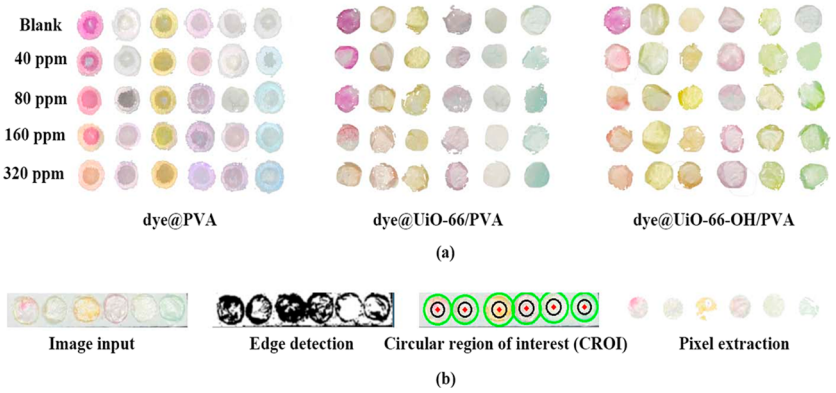

Figure 4. (a) Photos of the dye@UiO-66-OH/PVA sensor array exposed to methylamine gas as the gas concentration increased from 40 to 320 ppm. (b) Schematic of Hough transform ROI extraction processing.

https://doi.org/10.1021/acssensors.2c00255
ACS Sens. 2022, 7, 1847−1854

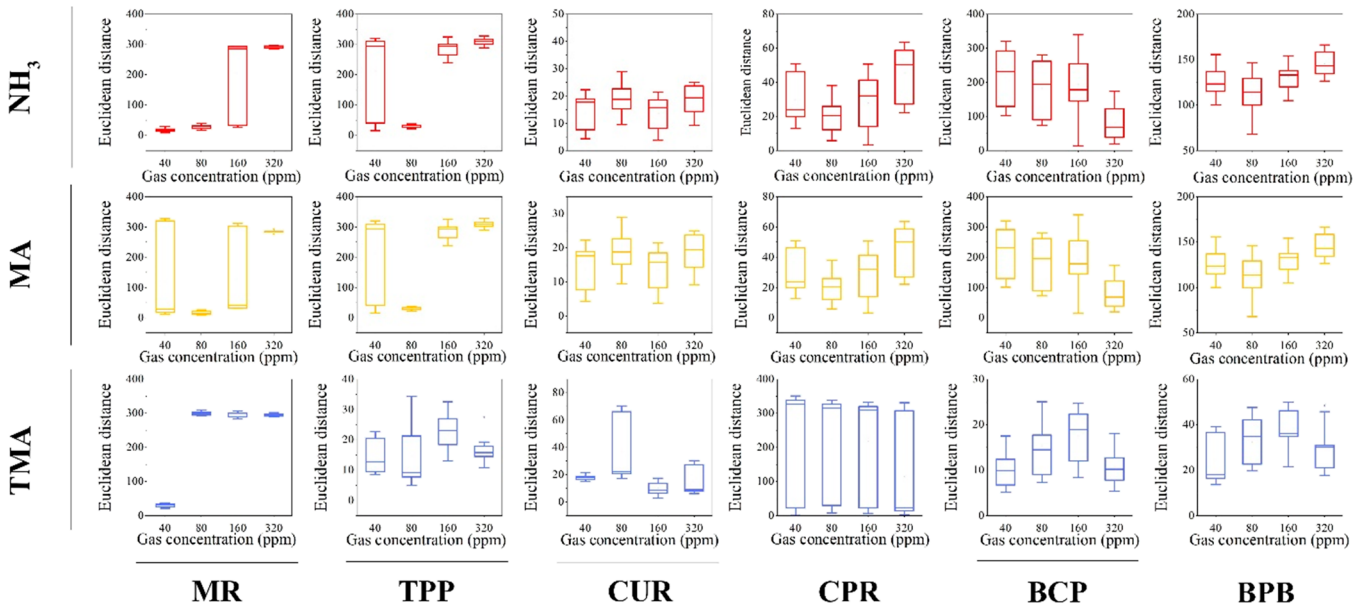

Figure 5. Boxplot of the ED distribution of different dyes based on UiO-66-OH/PVA MOF-MMM for NH_3, MA, and TMA at different gas concentrations (from 40 to 320 ppm, n = 10).

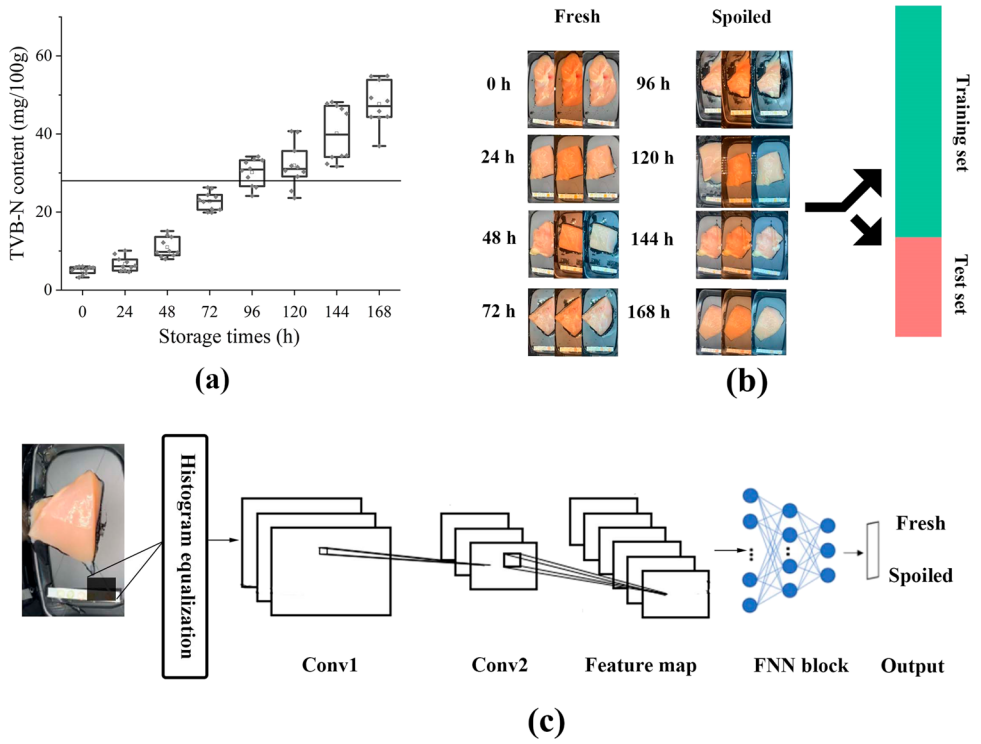

Figure 6. (a) Change in TVB-N content in a chicken breast sample during cold storage. (b) Chicken breast sample with sensor array image database structure. The database consisted of 4492 images for model training and 1927 for testing labeled with known TVB-N results. (c) DCNN models used for classification of chicken breast freshness.

in the storage environment. All the MOF-involved sensor arrays showed a significantly better response than dye@PVA, which was attributed to the three-dimensional porous structure of UiO-66 NPs, which enhanced gas transfer and brought more reaction sites (see the different scale of the y axis). The reflective effect in the figure was caused by the flatness of the sensor. Since we used the 3D printing mold and PVA was casted to form the film, the small-dimension PVA film naturally produced folds during drying and demolding. One of the most important advantages of neural networks is that they can extract important features from complex data sources. Moreover, as a result of DFT calculation, after being modified with a hydroxy group, the dye@UiO-66-OH/PVA sensor array showed a higher sensitivity than bare UiO-66, probably due to the low binding energy between UiO-66-OH and MA. Additionally, the limit of detection (LOD) of sensor arrays was calculated. Dye@UiO-66-OH/PVA showed the lowest LOD (80 ppm) and shortest equilibrium time (420 s), which

https://doi.org/10.1021/acssensors.2c00255
ACS Sens. 2022, 7, 1847−1854

was consistent with the previous results.[17] Based on the performance of the different sensor arrays, dye@UiO-66-OH/PVA was chosen for all subsequent experiments.

Deep Learning-Enabled Pattern Recognition Using DCNN. To make a prototype, we employed the newly constructed sensor array to identify the freshness of chicken. The chicken was frozen and stored at 4 °C in lunch boxes. The sensor arrays were photographed using an iPhone 11 max at various time intervals. According to a prior study, chicken with a TVB-N level lower than 28 mg/100 g was considered fresh, while those with a TVB-N value greater than 28 mg/100 g was declared spoiled and inedible.[16] The Conway technique was used to categorize the sensor array into these two freshness groups based on the TVB-N value of the chicken. Based on this criterion, the photographs were then classified as fresh or spoiled. Figure 6a depicts the general pattern of variations in TVB-N content throughout a 168 h cold storage period.

The dye@UiO-66-OH/PVA sensor arrays were fastened to the bottom of lunch boxes without coming into contact with the chicken samples. Every 24 h, the lunch box was moved out from the refrigerator and the cap was taken off before taking pictures in the photo box. To imitate the use of natural light for taking photos, the lighting conditions in the photo box were programmed in advance. After the sample was placed in the picture box, the light source's temperature and brightness were automatically modified. Following that, 6419 images of chicken breast with the sensor array were taken, resulting in a dataset for chicken freshness rating by machine learning. As indicated in the approach section, the dataset was first randomly split into a training subset (70%, or 4492 images) and a testing subset (30%, or 1927 images) (Figure 6b). The input, full connection, multiple convolutions, and output layers of a fresh/spoiled image classification network with distinct DCNN backbones were built. The trained DCNN extracted the features from images containing sensor arrays and chicken. Processed images were thereafter classified as either annotated 0 (fresh) or spoiled 1 (spoiled) (Figure 6c).

The ED value approach was used as a baseline to compare with the accuracy of deep learning models. Following our earlier study, we chose 50 sensor array pictures at random from the fresh and spoiled classes to test the accuracy of ED value prediction.[28] After all was said and done, the ED values had a prediction accuracy of 64.27%. When considering that this is a simple binary classification task (fresh/spoiled), this accuracy means that the method does not accomplish the task of freshness estimation. Thereafter, four cutting-edge DCNN models, Inception V3, VGG, Resnet-152, and WISsR-50, were applied for comparison. WISeR50 achieved the greatest accuracy for freshness classification, up to 98.95%, which was 34.68% higher than the ED value method. It is worth noting that this result was obtained while taking into consideration the extreme light conditions that we performed to interfere with the sample photographing. The accuracies of the other three deep learning algorithms are 97.28%, 97.46%, and 92.2% for VGG16, ResNet50, and Inception V3, respectively, which are all significantly higher than the baseline (Table 1).

To compare more precisely the performance of the different models, we plotted confusion matrices (Figure 7). For the four neural network models, the vast majority of the data was distributed within the diagonal lattice, which further corroborated the accuracy of the models calculated in the previous section. For three of these models (VGG16, WISeR50, and Inception V3), there were fewer false positives

Table 1. Accuracy Comparison Results between the ED Value Method and the Four DCNN Models

model	accuracy
Euclidean distance	64.27%
VGG16	97.28%
ResNet50	97.46%
WISeR50	98.95%
Inception V3	92.20%

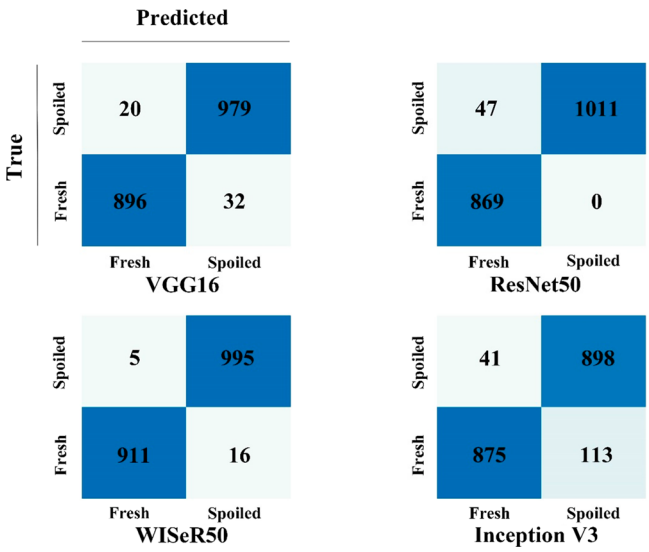

Figure 7. Confusion matrix of four DCNN models.

than false negatives. Considering the potential future application of the freshness sensor system to ensure food safety, false negatives are generally considered to be of greater concern. Here, it is found that the vast majority of trained neural nets tended to be more conservative in freshness analysis, thus further demonstrating their advantages. In the test dataset composed of 1927 photos, only 5 photos of spoiled chicken were classified as fresh by the WISeR50 model, accounting for only 0.26%.

Due to their higher accuracy, DCNN models may be preferable for colorimetric sensor array recognition and classification applications. Furthermore, there are a plethora of alternative sensor arrays that might benefit from the DCNN model while also promising to attain improved accuracy. The fundamental benefit of this technique is that it maintains a high level of picture classification accuracy while being simple to set up an image database. Meanwhile, the system can be applied to identify the freshness of other foods in the future by changing the image data set.

CONCLUSIONS

A unique MOF-MMM-based sensor array system was prepared for continuous, real-time, and non-destructive monitoring of chicken freshness. The system showed greatly improved water stability and sensitivity attributable to the incorporated UiO-66-OH NPs. Moreover, it effectively recognized gases emitted by spoiled chicken including NH_3, MA, and TMA and generated a fingerprint of the above VOCs. A deep learning-based image classification system was developed. All DCNN algorithms showed significantly higher accuracy than the ED value method, with the highest accuracy of 98.95% and lowest rate of false positive of 0.26% achieved by the WISeR50 model.

https://doi.org/10.1021/acssensors.2c00255
ACS Sens. 2022, 7, 1847−1854

The MOF-MMM-based sensor array approach has great potential to be embedded in smart packaging materials and monitor the freshness of food products.

■ ASSOCIATED CONTENT

Supporting Information

The Supporting Information is available free of charge at https://pubs.acs.org/doi/10.1021/acssensors.2c00255.

Table S1: List of biocompatible chromophore dyes used for the colorimetric sensor array; Table S2: Relative binding energy for NH_3, methylamine (MA) and trimethylamine (TMA) in meat and functionalized UiO-66 materials determined by periodic PBE-D2 calculations; Table S3: Particle size and zeta potential for UiO-66 and UiO-66-OH particles; Figure S1: X-ray diffraction (XRD) patterns of synthesized UiO-66-OH@PVA MMM, UiO-66, and UiO-66-OH compared with the simulated pattern for UiO-66 (PDF)

■ AUTHOR INFORMATION

Corresponding Author

Qin Wang − *Department of Nutrition and Food Science, College of Agriculture and Natural Resources, University of Maryland, College Park, Maryland 20742, United States;* orcid.org/0000-0002-7496-3921; Phone: 301-405-8421; Email: wangqin@umd.edu

Authors

Peihua Ma − *Department of Nutrition and Food Science, College of Agriculture and Natural Resources, University of Maryland, College Park, Maryland 20742, United States*

Wenhao Xu − *Department of Chemistry and Biochemistry, College of Computer, Mathematical and Natural Science, University of Maryland, College Park, Maryland 20742, United States*

Zi Teng − *Department of Nutrition and Food Science, College of Agriculture and Natural Resources, University of Maryland, College Park, Maryland 20742, United States; U. S. Department of Agriculture, Agricultural Research Service, Beltsville Agricultural Research Center, Food Quality Laboratory, Beltsville, Maryland 20705, United States;* orcid.org/0000-0002-6029-7024

Yaguang Luo − *U. S. Department of Agriculture, Agricultural Research Service, Beltsville Agricultural Research Center, Food Quality Laboratory, Beltsville, Maryland 20705, United States*

Cheng Gong − *Department of Electrical and Computer Engineering and Quantum Technology Center, University of Maryland, College Park, Maryland 20742, United States;* orcid.org/0000-0001-7714-6380

Complete contact information is available at: https://pubs.acs.org/10.1021/acssensors.2c00255

Notes

The authors declare no competing financial interest.

■ ACKNOWLEDGMENTS

The authors are grateful for the technical support of the Maryland NanoCenter at the University of Maryland. We thank the Chinese Scholarship Council for supporting P.M.'s learning and research.

■ REFERENCES

(1) Huang, X.; Zou, X.; Shi, J.; Li, Z.; Zhao, J. Colorimetric sensor arrays based on chemo-responsive dyes for food odor visualization. *Trends Food Sci. Technol.* **2018**, *81*, 90−107.

(2) Corradini, M. G. Shelf life of food products: from open labeling to real-time measurements. *Annu. Rev. Food Sci. Technol.* **2018**, *9*, 251−269.

(3) White, E. R.; Froehlich, H. E.; Gephart, J. A.; Cottrell, R. S.; Branch, T. A.; Baum, J. K. Early effects of COVID-19 interventions on US fisheries and seafood. **2020**. Van der Werf, P.; Gilliland, J. A. A systematic review of food losses and food waste generation in developed countries. In *Proceedings of the Institution of Civil Engineers-Waste and Resource Management*, 2017; Thomas Telford Ltd, Vol. *170*, pp. 66−77.

(4) Guo, L.; Wang, T.; Wu, Z.; Wang, J.; Wang, M.; Cui, Z.; Ji, S.; Cai, J.; Xu, C.; Chen, X. Portable Food-Freshness Prediction Platform Based on Colorimetric Barcode Combinatorics and Deep Convolutional Neural Networks. *Adv. Mater.* **2020**, *32*, 2004805.

(5) Yang, M.; Liu, X.; Luo, Y.; Pearlstein, A. J.; Wang, S.; Dillow, H.; Reed, K.; Jia, Z.; Sharma, A.; Zhou, B.; Pearlstein, D.; Yu, H.; Zhang, B. Machine learning-enabled non-destructive paper chromogenic array detection of multiplexed viable pathogens on food. *Nat. Food* **2021**, *2*, 110−117.

(6) Chen, J.; Chen, Z.; Boussaid, F.; Zhang, D.; Pan, X.; Zhao, H.; Bermak, A.; Tsui, C.-Y.; Wang, X.; Fan, Z. Ultra-low-power smart electronic nose system based on three-dimensional tin oxide nanotube arrays. *ACS Nano* **2018**, *12*, 6079−6088.

(7) Li, Z.; Li, H.; LaGasse, M. K.; Suslick, K. S. Rapid quantification of trimethylamine. *Anal. Chem.* **2016**, *88*, 5615−5620.

(8) Dechnik, J.; Gascon, J.; Doonan, C. J.; Janiak, C.; Sumby, C. J. Mixed-matrix membranes. *Angew. Chem., Int. Ed.* **2017**, *56*, 9292−9310.

(9) Cheng, W.; Tang, X.; Zhang, Y.; Wu, D.; Yang, W. Applications of metal-organic framework (MOF)-based sensors for food safety: Enhancing mechanisms and recent advances. *Trends Food Sci. Technol.* **2021**, *112*, 268−282. Zhang, Y.; Feng, X.; Yuan, S.; Zhou, J.; Wang, B. Challenges and recent advances in MOF−polymer composite membranes for gas separation. *Inorg. Chem. Front.* **2016**, *112*, 896−282.

(10) Kim, K. C.; Yu, D.; Snurr, R. Q. Computational screening of functional groups for ammonia capture in metal−organic frameworks. *Langmuir* **2013**, *29*, 1446−1456.

(11) Wu, Y.; Luo, Y.; Zhou, B.; Mei, L.; Wang, Q.; Zhang, B. Porous metal-organic framework (MOF) Carrier for incorporation of volatile antimicrobial essential oil. *Food Control* **2019**, *98*, 174−178.

(12) Cai, S.; Li, W.; Xu, P.; Xia, X.; Yu, H.; Zhang, S.; Li, X. In situ construction of metal−organic framework (MOF) UiO-66 film on Parylene-patterned resonant microcantilever for trace organophosphorus molecules detection. *Analyst* **2019**, *144*, 3729−3735.

(13) Abánades Lázaro, I.; Wells, C. J.; Forgan, R. S. Multivariate Modulation of the Zr MOF UiO-66 for Defect-Controlled Combination Anticancer Drug Delivery. *Angew. Chem., Int. Ed.* **2020**, *59*, 5211−5217.

(14) Ma, P.; Zhang, J.; Liu, P.; Wang, Q.; Zhang, Y.; Song, K.; Li, R.; Shen, L. Computer-assisted design for stable and porous metal-organic framework (MOF) as a carrier for curcumin delivery. *LWT* **2020**, *120*, No. 108949.

(15) Pounds, K.; Jairam, S.; Bao, H.; Meng, S.; Zhang, L.; Godinez, S.; Savin, D. A.; Pelletier, W.; Correll, M. J.; Tong, Z. Glycerol-Based Dendrimer Nanocomposite Film as a Tunable pH-Sensor for Food Packaging. *ACS Appl. Mater. Interfaces* **2021**, *13*, 23268−23281.

(16) Bekhit, A. E.-D. A.; Holman, B. W. B.; Giteru, S. G.; Hopkins, D. L. Total volatile basic nitrogen (TVB-N) and its role in meat spoilage: A review. *Trends Food Sci. Technol.* **2021**, 280.

(17) Ma, P.; Zhang, Z.; Xu, W.; Teng, Z.; Luo, Y.; Gong, C.; Wang, Q. Integrated Portable Shrimp-Freshness Prediction Platform Based on Ice-Templated Metal−Organic Framework Colorimetric Combinatorics and Deep Convolutional Neural Networks. *ACS Sustainable Chem. Eng.* **2021**, 16926−16936.